



OPA1 Mutation and Late-Onset Cardiomyopathy: Mitochondrial Dysfunction and mtDNA Instability

Le Chen, Tingting Liu, Alice Tran, Xiyuan Lu, Alexey A. Tomilov, Vanessa Davies, Gino Cortopassi, Nipavan Chiamvimonvat, Donald M. Bers, Marcela Votruba and Anne A. Knowlton

J Am Heart Assoc. 2012;1:e003012; originally published October 8, 2012;

doi: 10.1161/JAHA.112.003012

The *Journal of the American Heart Association* is published by the American Heart Association, 7272 Greenville Avenue, Dallas, TX 75231
Online ISSN: 2047-9980

The online version of this article, along with updated information and services, is located on the World Wide Web at:

<http://jaha.ahajournals.org/content/1/5/e003012>

Data Supplement (unedited) at:

<http://jaha.ahajournals.org/content/suppl/2012/10/05/1.5.e003012.DC1.html>

Subscriptions, Permissions, and Reprints: The *Journal of the American Heart Association* is an online only Open Access publication. Visit the Journal at <http://jaha.ahajournals.org/> for more information.

OPA1 Mutation and Late-Onset Cardiomyopathy: Mitochondrial Dysfunction and mtDNA Instability

Le Chen, MD, PhD; Tingting Liu, BS; Alice Tran, BS; Xiyuan Lu, MS; Alexey A. Tomilov, PhD; Vanessa Davies, PhD; Gino Cortopassi, PhD; Nipavan Chiamvimonvat, MD; Donald M. Bers, PhD; Marcela Votruba, MD, PhD, FRCOphth; Anne A. Knowlton, MD

Background—Mitochondrial fusion protein mutations are a cause of inherited neuropathies such as Charcot–Marie–Tooth disease and dominant optic atrophy. Previously we reported that the fusion protein optic atrophy 1 (OPA1) is decreased in heart failure.

Methods and Results—We investigated cardiac function, mitochondrial function, and mtDNA stability in a mouse model of the disease with OPA1 mutation. The homozygous mutation is embryonic lethal. Heterozygous OPA^{+/-} mice exhibit reduced mtDNA copy number and decreased expression of nuclear antioxidant genes at 3 to 4 months. Although initial cardiac function was normal, at 12 months the OPA^{+/-} mouse hearts had decreased fractional shortening, cardiac output, and myocyte contraction. This coincided with the onset of blindness. In addition to small fragmented mitochondria, aged OPA^{+/-} mice had impaired cardiac mitochondrial function compared with wild-type littermates.

Conclusions—OPA1 mutation leads to deficiency in antioxidant transcripts, increased reactive oxygen species, mitochondrial dysfunction, and late-onset cardiomyopathy. (*J Am Heart Assoc.* 2012;1:e003012 doi: 10.1161/JAHA.112.003012)

Key Words: cardiomyopathy • mitochondrial fusion • mtDNA • OPA1 • ROS

Mitochondria were long viewed as vital but static energy factories; however, mitochondria have been found to be dynamic organelles that not only continuously divide and fuse within the cell, but also have functions extending beyond energy production to cell signaling.^{1,2} Complete mitochondrial fusion requires 2 steps, in which the outer and inner mitochondrial membranes fuse in separate events.² The mitofusins MFN1 and MFN2 are on the mitochondrial outer membrane and are involved in the first step of mitochondrial fusion, whereas optic atrophy 1 (OPA1) fuses the inner membrane. On the other hand, mitochondrial fission is controlled by Fis1 and DRP1 in mammalian cells. The rate of fission and fusion in mammalian cells is thought to be much

slower than that in simpler organisms such as yeast, in which fusion and fission were first described.³

Recent studies have explored whether maintaining overall mitochondrial morphology and function relies on preserving the balance of fusion and fission. Imbalanced mitochondrial fusion/fission leads to apoptosis, mitochondrial DNA (mtDNA) mutations, and a severe reduction in respiratory capacity.^{1,4} There are a number of inherited neuropathies such as Charcot–Marie–Tooth disease and dominant optic atrophy that cause neuropathy and blindness. Several of these diseases have been shown to be caused by mutation of MFN2⁵ and OPA1.^{6,7} Abnormal expression of MFN2 has also been found in other diseases including Parkinson's disease and type 2 diabetes.¹

The heart, like the brain, has a high demand for ATP and is dependent on mitochondrial high-energy phosphate production. However, only limited studies have addressed whether mitochondrial fusion/fission abnormalities have a role in heart failure. We have previously reported that OPA1⁸ is decreased in both human and rat heart failure. Electron microscopic analysis showed increased number and decreased size of mitochondria, consistent with depressed mitochondrial fusion, in a high coronary artery ligation rat heart failure model. However, it remains unknown whether this reduction of mitochondrial fusion is secondary to heart failure or a contributor to the development and progression of heart failure. Investigation has been limited on the role of

From the Departments of Medicine (L.C., T.L., A.T., N.C., A.A.K.), Pharmacology (X.L., D.M.B., A.A.K.), and Molecular Biosciences (A.A.T., G.C.), University of California, Davis, CA; School of Optometry & Vision Sciences, Cardiff University, Cardiff, UK (V.D., M.V.); Northern California VA, Sacramento, CA (N.C., A.A.K.).

Accompanying tables S1–S3 are available at <http://jaha.ahajournals.org/content/1/5/e003012.full>

Correspondence to: Anne A. Knowlton, MD, Molecular & Cellular Cardiology, University of California, Davis, One Shields Avenue, Davis, CA 95616. E-mail: aaknowlton@ucdavis.edu

Received June 22, 2012; accepted July 31, 2012.

© 2012 The Authors. Published on behalf of the American Heart Association, Inc., by Wiley-Blackwell. This is an Open Access article under the terms of the Creative Commons Attribution Noncommercial License, which permits use, distribution, and reproduction in any medium, provided the original work is properly cited and is not used for commercial purposes.

OPA1-mediated mitochondrial fusion in the heart. There also remain concerns whether mitochondrial dynamic changes occur readily in cardiac muscle fibers, where mitochondria are highly organized and compacted between contractile filaments or adjacent to the sarcolemma. However, given the heart's high energy requirements, it seems very likely that changes in fusion proteins would have a negative impact on cardiac function.

To address our hypothesis that loss of fusion proteins contributes to the development of cardiomyopathy, we studied mice with an OPA1 mutation, modeling dominant optic atrophy. We found that these mice had a late onset of cardiomyopathy. Furthermore, reduction in OPA1 led to abnormalities in mitochondrial organization, depressed mitochondrial respiration, and increased mtDNA deletion, as well as increased reactive oxygen species (ROS).

Experimental Procedures

Mouse Breeding

OPA1 mutation has been generated as previously described; the introduced stop codon is at the beginning of the dynamin GTPase, a domain where many human disease-causing mutations cluster.⁹ OPA1^{+/-} mice and littermate controls were bred by crossing OPA1^{+/-} and WT C57Bl/6JCrI (Charles River). This has been continuing from G2 to G16 (currently). Animals aged 3 to 4 months (3 months) and 12 to 14 months (12 months) were used. All experiments were approved by the Institutional Animal Care and Use Committee at UC Davis.

Cardiac Functional Measurements

Echocardiography

In all, 6 to 7 age- and sex-matched WT and OPA1^{+/-} mice were examined at different ages (monthly). Murine transthoracic echocardiography was conducted in conscious mice as previously described.¹⁰ Briefly, the heart was imaged in a 2-dimensional parasternal short-axis view with M-mode echocardiogram of the midventricle recorded at the level of the papillary muscle. Left ventricle (LV) fractional shortening was calculated as previously described.¹⁰

Hemodynamics measurements

Hemodynamics measurements were performed as previously described.¹¹ Briefly, a lateral thoracotomy was done, and a 2.0 f Millar catheter was passed through the left carotid artery into the left ventricular chamber. Hemodynamic function was measured, including volume loops and cardiac output.

Cardiomyocyte contractility and calcium transients

Cardiomyocyte contractility and calcium transients were synchronously detected using an IonOptix system (IonOptix, Milton, MA) as previously described.¹²

Histological and Electron Microscopy Analysis

The left ventricle was used for histological analysis. COX/SDH staining was performed according to the method of Chen et al.¹³ Freshly dissected heart tissue was embedded in Optimal Cutting Temperature (OCT) compound (Tissue-Tek) and frozen in liquid nitrogen. Slides were stained for COX activity, washed in water, stained for SDH activity, washed, and mounted in GelMount (Biomedica). For electron microscopy (EM), mouse hearts were fixed with 4% paraformaldehyde and then processed and imaged as described previously.⁸

Respiration Measurements

Oxygen consumption was measured in freshly isolated cardiac mitochondria using the XF24 Seahorse instrument, modified based on a previously described method.¹⁴ State II respiration was initiated by adding substrate — 5 mmol/L succinate in the presence of 2 μ mol/L rotenone. State III respiration was measured by the addition of ADP to a final concentration of 2.5 mmol/L. Uncoupled respiration rates were determined by injection of 2.5 μ mol/L mesoxalonnitrile 4-trifluoromethoxyphenylhydrazine (FCCP). State IV respiration was measured following ADP consumption. Respiration due to proton leak was determined using 0.5 μ mol/L oligomycin.

Complex I, II, and IV activities were measured in freshly isolated mitochondrial lysates following the recommendations of the manufacturer (Mitoscience) as previously reported.¹⁵

ATP Production Rates in Isolated Heart Mitochondria

ATP synthesis rates in isolated heart mitochondria were determined using the luciferin/luciferase-based ATP Bioluminescence Assay Kit (Sigma) essentially as described.¹⁶ Basal ATP content in heart left ventricle tissue was directly measured using tissue lysate. For complex I-driven ATP synthesis, 5 to 10 μ g of heart mitochondria was dissolved in 50 μ L of buffer A (125 KCL, 10 mmol/L HEPES, 5 mmol/L MgCl₂, and 2 mmol/L K₂HPO₄, pH 7.44) plus complex I substrate pyruvate/malate, 5 mmol/L final, with and without 2 mmol/L rotenone. The ATP measurements in the presence of rotenone were subtracted to give ATP production via complex I. The measurements for all samples were started simultaneously by adding 50 μ L of luciferin/luciferase buffer containing 1 mmol/L ADP (0.5 mmol/L final). Using an ATP

standard provided in the kit, the slopes were converted to nanomoles per minute per milligram of protein.

DNA Isolation

To isolate mtDNA, mouse left ventricles were first homogenized, and a mitochondrial fraction was isolated according to previously published protocols.¹³ Mitochondria were then lysed in the presence of 0.5% SDS and 0.2 mg/mL proteinase K in 10 mmol/L Tris-HCl, 0.15 mol/L NaCl, and 0.005 mol/L EDTA. mtDNA was then extracted and purified with Dynabeads (Invitrogen). Total DNA was isolated using standard protocols.

mtDNA Quantitation

To quantify the amount of mtDNA present per nuclear genome, we used the primers as listed in Table S3. All samples were measured in triplicate, and qPCR results obtained were confirmed by 3 independent experiments. Two different primer pairs were used to quantify and confirm relative mtDNA copy number as previously described¹⁴: COXI and cytochrome b (mitochondrial) and β -globin/H-19 for genomic DNA. Data obtained by qPCR were analyzed by the $\Delta\Delta$ CT method.

Apoptosis Assays

TUNEL staining was performed on heart sections using a commercial kit (In Situ Cell Death Detection Kit, Roche) following the manufacturer's instructions. Percentage of TUNEL positive cells was calculated as previously described.⁸

Western Blotting

The left ventricle was homogenized in RIPA buffer as previously described.⁸ Fifty micrograms of lysate was electrophoresed and transferred to nitrocellulose membranes. Blots were blocked with 5% nonfat dry milk and incubated overnight at 4°C with anti-TFAM, PGC1- α , MFN1, MFN2, Bax, Bak, and Nrf2 antibodies (Abcam, 1:1000); GAPDH was used as an internal control. Blots then were washed and incubated with secondary antibodies (1/10 000 goat anti-rabbit-HRP/anti-mouse-HRP, GE) and developed with the Femto chemiluminescent reagent (Pierce).

ROS Assays

ROS level was measured by a fluorescent method with confocal microscopy. CellROX deep red (Invitrogen) was used as indicator of cell ROS. Cardiomyocytes were isolated as previously described,¹⁶ and myocytes were incubated with CellROX at 37°C for 30 minutes. Nuclei indicator DAPI was

used as a counterstain. The intensity of CellROX fluorescence was calculated and analyzed to quantify the ROS level. One hour of hypoxia followed by 1 hour of reoxygenation was performed using standard protocols as previously described.⁸ Total antioxidant capacity (TAC) was measured using a TAC ELISA kit (Cell Biolabs) following the manufacturer's protocol. Briefly, left ventricles were homogenized and centrifuged at 10 000g for 10 minutes at 4°C. One hundred milligrams of supernatant was loaded into a 96-well plate for subsequent TAC assay. After 30 minutes' incubation with copper ion reagent, the reduction of copper(II) to copper(I) by anti-oxidants was measured for absorbance at 490 nm.

PCR Array

Total RNA was extracted from mouse left ventricle by the standard Trizol (Invitrogen) method, and PCR array was performed following the manufacturer's protocol. Mitochondrial gene and stress-related gene PCR arrays (Qiagen) were used to determine the gene profile changes in OPA1-mutant hearts. Data obtained by qPCR were analyzed by the $\Delta\Delta$ CT method.

Statistical Analysis

Results are expressed as mean \pm SEM. Results from multiple groups were compared by analysis of variance (ANOVA) followed by a Student–Neuman–Keuls test for multiple comparisons. The Student *t* test was used for comparisons involving only 2 groups. The Wilcoxon rank-sum test and Kruskal–Wallis ANOVA were performed when data were not normally distributed. A *P*<0.05 was considered significant. In PCR array analysis, *q* value was calculated using Q-Value software (<http://genomics.princeton.edu/storeylab/qvalue/>). A limitation of the study was the relatively small sample size for some experiments.

Results

Abnormal Cardiac Function in OPA1 Mutants at 12 Months

An *OPA1* gene mutation, B6;C3-Opa1(Q285STOP), which models autosomal dominant optic atrophy, was generated in the mouse.⁹ The homozygous mutation is embryonic lethal, whereas the heterozygous mutation is associated with visual dysfunction and structural changes in the murine retina and optic nerve beginning at 12 months.⁹ The animals looked vigorous and appeared healthy. Initial descriptive studies of the heart showed no abnormalities, but specialized techniques are needed to detect many significant cardiac abnormalities. The heterozygote has a 50% reduction in the

OPA1 transcript and protein in the mouse heart (Figure 1a). Given the unique arrangement of mitochondria in cardiac muscle, we examined whether OPA1 and mitochondrial fusion play an important role in this tissue. Although no significant changes in the heart weight/tibia length ratio occurred at 3 months, heart weight and chamber size were mildly decreased after 12 months in the OPA1 mutants (Figure 1b and 1c). Cardiac function was assessed monthly by echocardiogram beginning at 3 months of age in OPA1^{+/-} mice. No significant cardiac functional or gross structural abnormalities were found in these mice until 12 months, when significantly

impaired contraction developed. Fractional shortening (FS) dropped from 74.18±1.81% to 47.87±2.75% ($P<0.05$) at 12 months in OPA1 mutants but did not change in WT hearts, nor in OPA1 mutants at 3 months, as shown in Figure 1d through 1f. There was no statistical difference in cardiac left ventricular end diastolic dimension (LVEDD) between the OPA1-mutant and WT groups (Figure 1g). Invasive hemodynamic studies at 12 months showed abnormal pressure–volume loops in OPA1^{+/-} mice compared with WT littermates (Figure 2a). The pressure–volume loops were mildly narrowed, consistent with decreased cardiac output in the OPA1^{+/-} hearts. Most importantly, much less pressure was generated by the OPA1^{+/-} hearts with contraction (Figure 2a). LVDPmax was significantly decreased in OPA1^{+/-} hearts compared with WT (Figure 2b), whereas there was no statistical difference in the left ventricular end diastolic

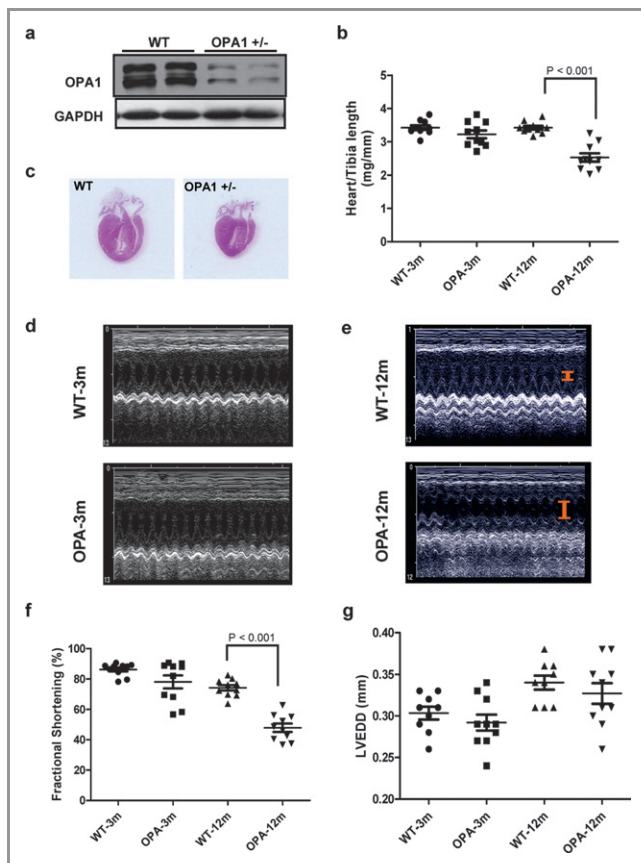


Figure 1. Cardiac OPA1 levels, gross cardiac morphology, and cardiac dysfunction in the OPA1^{+/-} mouse. a, OPA1 is reduced 50% in the heterozygote heart. b, Heart weight/tibia length ratio indicates the heart is slightly smaller in the mutants at 12 months (n=10 per group). c, H & E staining of representative coronal sections of the heart showing the 4 chambers from mutant and WT at 12 months. Cardiac echo from 3 to 4 months (d) and 12 months (e) mice. f, Decreased fractional shortening was evident at 12 months in the OPA1 mutants (n=10 per group). g, Left ventricular end-diastolic dimension (LVEDD, d) did not differ among groups, showing that no ventricular dilatation was present despite decline in OPA1 heterozygote heart function at 12 months (n=10 per group). WT indicates wild-type; OPA, OPA1^{+/-}; 3 m, 3 to 4 months; 12 m, 12 months. Data are represented as mean±SEM, and ANOVA was used to calculate the statistical significance.

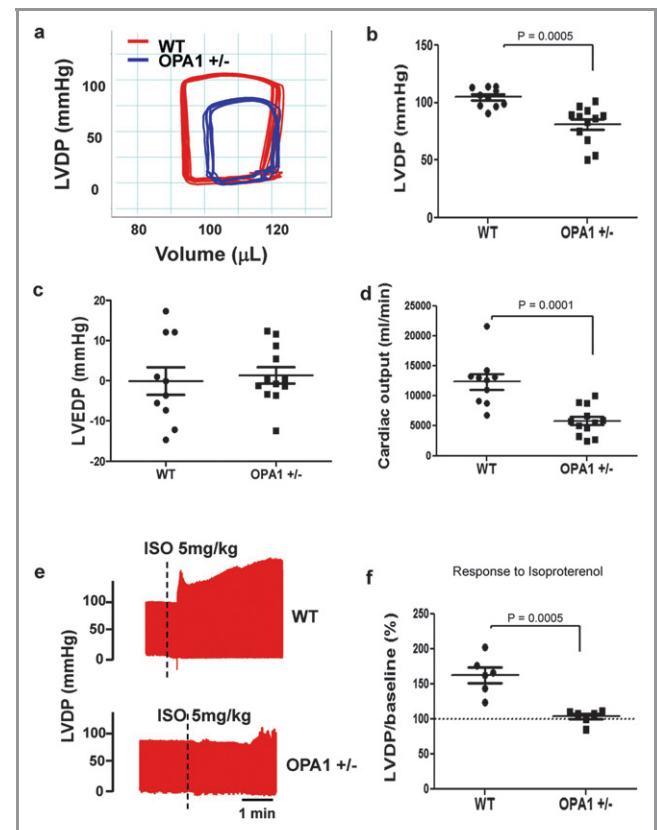


Figure 2. OPA1 mutation associated with impaired hemodynamics at 12 months. a, At 12 months, OPA1^{+/-} mice had abnormal pressure–volume loops compared with WT littermates. b, Left ventricular developed pressure (LVDP) was decreased at 12 months in the mutant hearts (n=10 to 12 per group). c, Cardiac output was significantly depressed at 12 months in the OPA1-mutant heart (n=10 to 12 per group). d and e, Depressed response to beta agonist – OPA1^{+/-} hearts showed markedly less response to β stimulus (isoproterenol), consistent with reduced cardiac inotropy (n=6 per group). Data are represented as mean±SEM, and the *t* test was used to calculate statistical significance.

pressure (LVEDP, Figure 2c). Cardiac output was markedly reduced in OPA1 mutants, from 12.37 ± 1.87 to 5.82 ± 0.70 mL/min ($P < 0.001$), compared with WT (Figure 2d). Cardiac inotropic reserve was tested with the β -adrenergic agonist isoproterenol using a standard protocol. The 12-month OPA1^{+/-} hearts showed little to no response to β -adrenergic stimulus compared with WT (Figure 2e and 2f).

Calcium flux is a critical component of contractility. In isolated cardiomyocytes, 12-month OPA1 mutants had markedly reduced amplitudes of both calcium transients and contraction (Figure 3), and calcium transient decline and myocyte relaxation exhibited slowed kinetics. These changes recapitulate the cardiac dysfunction observed at the organ level and demonstrate that dysfunction at the individual myocyte level, rather than loss of myocytes per se, may be critical in overall OPA1-mutant dysfunction.

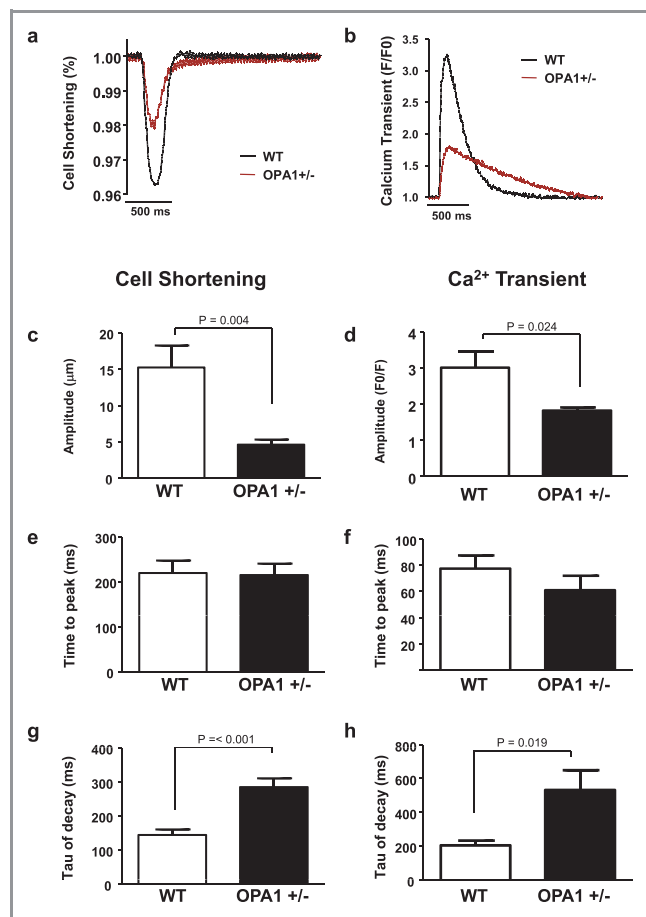


Figure 3. Cell shortening and calcium transients. Representative traces show depressed cell shortening (a) and calcium transients (b) in old OPA1-mutant cardiomyocytes. Amplitude, time to peak, and decay of cell shortening (c, e, and g) and calcium transients (d, f, and h) all were consistent with decreased contractility of cardiomyocytes from old OPA1 mutants. Data are represented as mean ± SEM (n=9 to 10 per group). The *t* test was used to calculate statistical significance.

Mitochondrial Structure and Function

Electron microscopy

EM was used to investigate cellular structure in the left ventricle (Figure 4). The young WT heart showed orderly

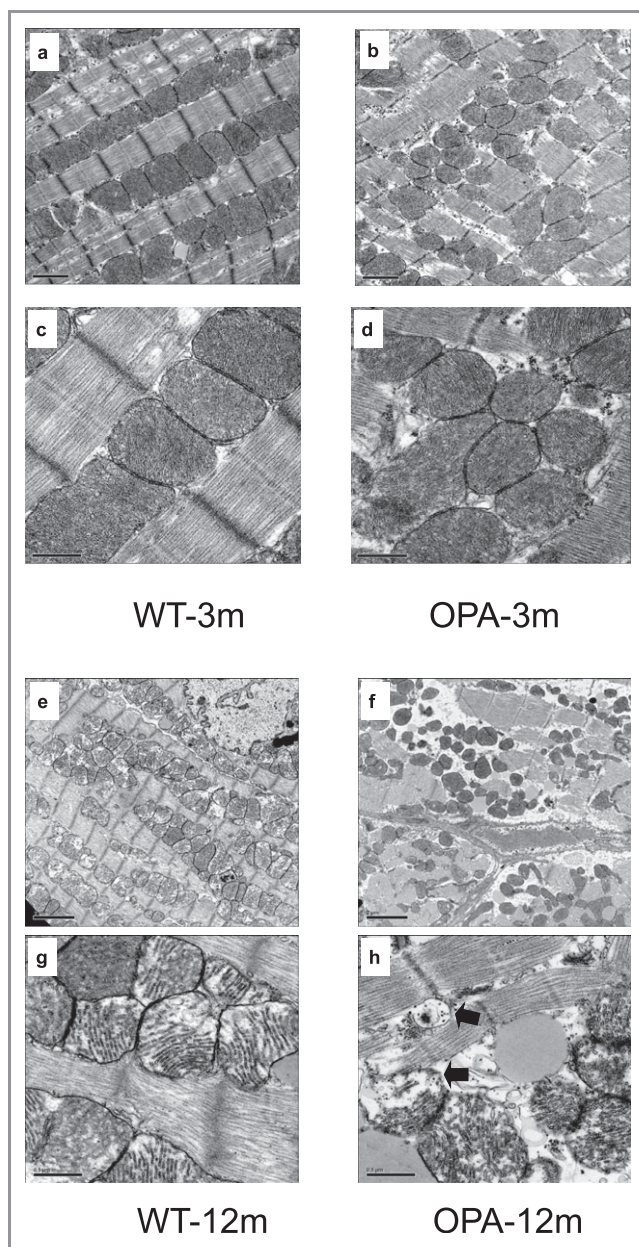


Figure 4. Electron microscopy of OPA1^{+/-} and WT left ventricles (a through d: 3 months; e through h: 12 months) demonstrating mitochondria losing order and separating from each other at both 3 and 12 months, which is likely to be loss of mitochondrial fusion in OPA1^{+/-} hearts (b, d, f, h) compared with WT (a, c, e, g). Higher-magnification images show mitochondria with loss of the normal mitochondrial cristae structure (indicated by arrows) at 12 months in OPA1 mutants (h) compared with WT (g), suggested incomplete mitochondrial respiratory function. WT indicates wild type; OPA, OPA1^{+/-}; 3 m, 3 to 4 months; 12 m, 12 months.

arrays of mitochondria between myofilaments (Figure 4a and 4c). This pattern was not found in OPA1^{+/-} hearts (Figure 4b and 4d). The OPA1^{+/-} hearts had greater disruption of mitochondrial organization along with decreased density of mitochondria/area, suggesting of loss of mitochondria (Figure 4c and 4d). Higher magnification (Figure 4g and 4h) revealed damage to the normal mitochondrial cristae structure with loss of cristae, consistent with impaired mitochondrial respiratory function. The WT cardiac mitochondria showed normal alignment along the sarcomere, but there was some loss of cristae at 12 months (Figure 4e and 4g), likely from aging.¹⁷

Mitochondrial function

Enzyme activities for complexes I, II, and IV were measured in vitro in WT and OPA1^{+/-} mouse hearts. Fresh cardiac mitochondrial lysates were prepared and complex enzyme activities measured using a 96-well plate-based assay (Mitosciences, Eugene, OR). Activities of complexes I and IV decreased significantly in OPA1^{+/-} hearts, whereas complex II activity remained unchanged compared with WT (Figure 5a through 5c). Direct mitochondrial respiration studies using freshly isolated mitochondria from OPA1^{+/-} and WT left ventricles were done to complement the in vitro assays of complex function. Depressed oxygen consumption was detected both in succinate/ADP-driven state III respiration and in FCCP-induced maximal respiration capacity in the 12-month OPA1^{+/-} cardiac mitochondria, whereas no difference was found in the young (Figure 5d). Consistent with these findings, basal cardiac ATP content in left ventricular tissue lysate was significantly decreased in the aged OPA1^{+/-} compared with aged WT hearts ($P < 0.05$). A more modest but significant decrease in ATP occurred in the aged WT ($P < 0.05$; Figure 5e). Complex I-driven ATP synthesis was measured in freshly isolated cardiac mitochondria, and there was a significant decrease in ATP synthesis in aged OPA1^{+/-} hearts, whereas no statistical differences were found in the young groups ($P < 0.01$; Figure 5f). These results suggest that OPA1 plays a critical role in maintaining mitochondrial respiration and sustaining mitochondrial energy production at 12 months, which are known to be defective in heart failure.

Mitochondrial DNA

Given the ultrastructural and functional evidence for mitochondrial dysfunction, we first assessed mitochondrial-encoded versus nuclear-encoded mitochondrial protein activity using traditional histochemical staining for cytochrome c oxidase (COX, complex IV, brown stain) and succinate dehydrogenase (SDH, complex II, blue stain). In both 3- and

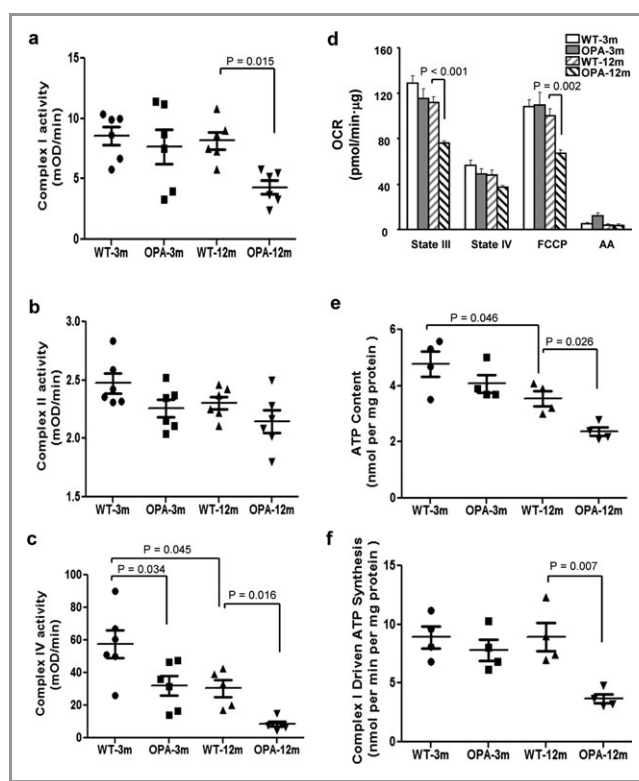


Figure 5. Mitochondrial dysfunction in OPA1-mutant hearts. a through c, Enzyme activities of complex I, II, and IV measured in WT and OPA1^{+/-} mouse hearts (n=6 to 7 per group). d, Oxygen consumption rates (OCR) in WT and OPA1^{+/-} heart mitochondria in the presence of succinate. State III was induced by injection of ADP. State IV was induced by inhibition of ATP synthase with oligomycin, and uncoupled respiration rates were determined by injection of mesoxalonyl 4-trifluoromethoxyphenylhydrazone (FCCP). Antimycin A (AA) was used to determine background, nonmitochondrial OXPHOS, OCR (n=7 to 8 per group). e, Basal ATP content (n=4 per group). f, Complex I-driven ATP synthesis measured in freshly isolated cardiac mitochondria in the presence of the complex I substrate pyruvate/malate, with and without rotenone. The ATP measurements in the presence of rotenone were subtracted to give ATP production via complex I. WT (n=4 per group) indicates wild type; OPA, OPA1^{+/-}; 3 m, 3 to 4 months; 12 m, 12 to 14 months. Data are represented as mean±SEM, and ANOVA was used to calculate statistical significance.

12-month wild-type mice, the cardiac sections showed predominantly brown COX staining of the cardiac fibers (Figure 6a, 1 and 3). However, in OPA1-mutant hearts, the staining pattern in both groups was predominantly blue, indicating reduced COX activity (Figure 6a, 2 and 4). This characteristic abnormal blue histological pattern is often found in cases of respiratory dysfunction due to mtDNA defects,^{13,18} because SDH activity is encoded solely by the nuclear genome, whereas COX activity is dependent on the mitochondrial genome. The decreased COX staining is consistent with the reduction of mitochondrial complex IV enzyme activity in the OPA1-mutant hearts (Figure 5c).

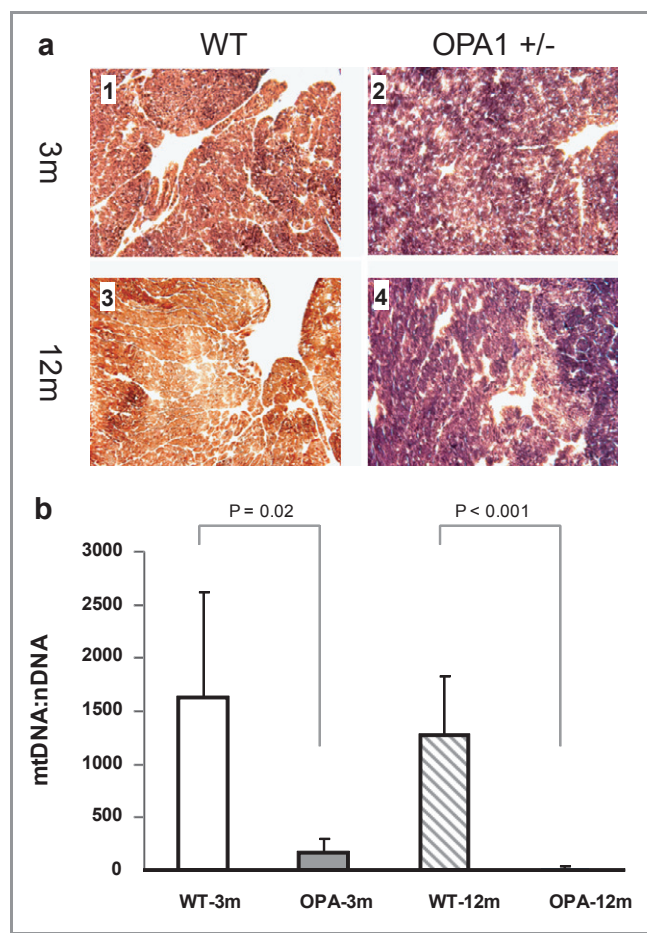


Figure 6. Loss of mtDNA stability in OPA1-mutant hearts. a, Transverse sections of the left ventricle were stained for COX (brown) and SDH (blue) activity. Blue staining indicates mitochondrial dysfunction (reduction in COX) and mtDNA deletion. b, Quantitative analysis of cardiac mtDNA copy number per nuclear genome at 3 and 12 months (n=4 to 5 per group). WT indicates wild type; OPA, OPA1^{+/-}; 3 m, 3 to 4 months; 12 m, 12 to 14 months. Data are represented as mean±SEM, and ANOVA was used to calculate statistical significance.

Real-time PCR was employed to more precisely investigate mtDNA copy number using the approach described by Sahin et al.¹⁴ Despite the lack of grossly abnormal pathology or function for the young OPA1 hearts, mtDNA copy number was markedly reduced compared with WT littermates (Figure 6b). The OPA1-mutant hearts had even greater reduction in mtDNA copies per nuclear genome at 12 months (Figure 6b). The mtDNA loss in this case is not likely related to mitochondrial biogenesis because PGC-1 α and TFAM protein content was unchanged (Figure 7).

OPA1 Mutation and Oxidative Stress

Studies of ROS in OPA1-mutant cardiomyocytes showed increased resting ROS compared with WT controls (Figure 8a

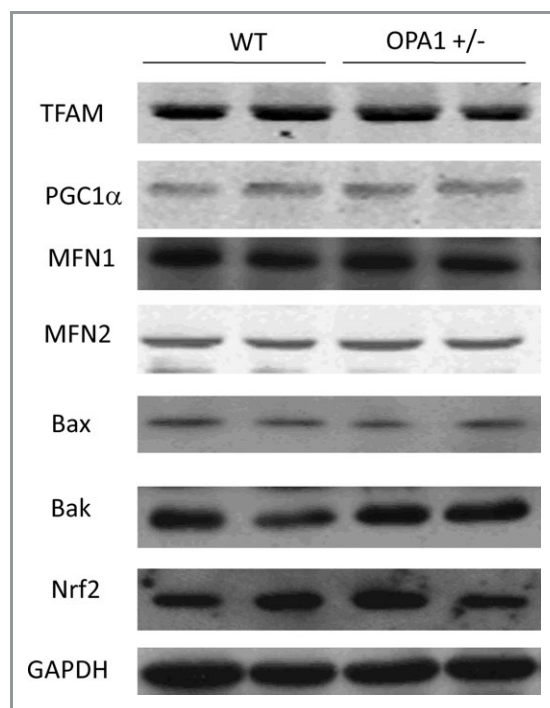


Figure 7. Expression of key proteins in OPA1^{+/-} vs WT hearts at 12 months. Western blots showing unchanged TFAM, PGC1- α , MFN1, MFN2, Bax, Bak, and Nrf2 in OPA1-mutant hearts. GAPDH was used as a loading control.

and 8b) at 12 months, indicating reduced ability to handle ROS in OPA1-mutant hearts. A PCR array focused on oxidative stress-related genes demonstrated a marked reduction in the number of antioxidant genes, both at young and older ages, in the OPA1-mutant heart (Table 1, the entire list can be found as Table S1). Downregulated antioxidant enzymes included Gpx3 and Gstk1. In the young OPA1-mutant heart, the DNA repair-related gene *Ercc6* and the oxidative stress mediator protein Txnip were upregulated. These results suggest that OPA1 mutants may be more vulnerable to ROS-inducing factors such as ischemia/reperfusion. At 3 months, both OPA1-mutant and WT myocytes showed low basal ROS levels. After 1 hour of hypoxia and 1 hour of reoxygenation, both mutant and WT young myocytes had increased ROS levels, but levels from the mutant myocytes were strikingly increased compared with WT myocytes (Figure 9). Moreover, by using a cell Live/Dead assay (Invitrogen), it was found that 6 hours of hypoxia and 1 hour of reoxygenation induced significantly more cell death in young OPA1-mutant cardiomyocytes compared with WT myocytes ($P < 0.001$, Figure 10), indicating greater vulnerability to ROS stress in the OPA1-mutant heart. In addition, total antioxidant capacity was reduced significantly in both young and older OPA1-mutant hearts compared with WT hearts (Figure 8c).

Table 1. Summary of Transcriptional Regulation of Oxidative Stress–Related Genes

Gene	Description	Function	Fold Induction	P
WT vs OPA1 ^{+/-} (3 to 4 months)				
<i>Ercc6</i>	Excision repair cross-complementing rodent repair deficiency, complementation group 6	DNA repair	1.88	0.044
<i>Txnip</i>	Thioredoxin interacting protein	Oxidative stress mediator	2.29	0.028
<i>Gpx2</i>	Glutathione peroxidase 2	Antioxidants	-3.34	0.014
<i>Gpx3</i>	Glutathione peroxidase 3	Antioxidants	-3.10	0.038
<i>Gstk1</i>	Glutathione S-transferase kappa 1	Antioxidants	-2.16	0.038
<i>Txnrd2</i>	Thioredoxin reductase 2	Antioxidants	-5.01	0.047
WT vs OPA1 ^{+/-} (12 months)				
<i>Cyba</i>	Cytochrome b-245, alpha polypeptide	Antioxidants	-1.31	0.028
<i>Gpx3</i>	Glutathione peroxidase 3	Antioxidants	-2.67	0.007
<i>Gstk1</i>	Glutathione S-transferase kappa 1	Antioxidants	-1.63	0.024
<i>Prdx6-rs1</i>	Peroxioredoxin 6, related sequence 1	Antioxidants	-3.41	0.021
<i>Srxn1</i>	Sulfiredoxin 1 homolog (<i>Saccharomyces cerevisiae</i>)	Antioxidants	-2.63	0.039

Positive value indicates upregulation; negative value, downregulation; WT, wild type; and OPA1, optic atrophy 1.

OPA1 Mutation and Apoptosis

Although OPA1-mediated mitochondrial fusion has been linked to protection from apoptosis,¹⁹ there was no statistical difference in TUNEL-positive cells or histological evidence of cardiac myocyte loss in OPA1-mutant hearts (Figure 11). There were no statistical differences found in mitochondrial intrinsic apoptosis-related genes, including *Bak1*, *Bcl2*, *Bcl2l1*, and *Bnip3* (Table S2). In addition, no difference was detected in the proapoptotic Bak and Bax proteins (Figure 7).

Discussion

Homozygous null mutations of OPA1 are embryonic lethal.⁹ The heterozygote had slow development of cardiomyopathy, characterized by reduced fractional shortening, markedly reduced inotropy, abnormal calcium transients, mitochondrial dysfunction leading to reduced ATP levels, decreased antioxidant gene expression, and increased ROS. However, despite these many changes, we detected no increase in apoptosis. mtDNA copy number was strikingly reduced, and this certainly contributed to some of the abnormalities, including complex IV dysfunction through reduction of COX expression. Interestingly, the onset of eye disease⁹ and cardiomyopathy occurred simultaneously at 12 months. These findings suggest a progressive pathological process induced by OPA1 reduction. Although there are some changes with aging in the WT, leading to mild reduction in ATP content and mitochondrial ultrastructure, the OPA1 mutant has far more dramatic effects on mitochondrial morphology and function.

Recently, Dorn et al reported that silencing of OPA1 and mitochondrial assembly regulatory factor (MARF) induces heart tube dilation in a *Drosophila* model.²⁰ In another report, a different OPA1 splicing mutation, which leads to an in-frame deletion of 27 amino acid residues in the GTPase domain, showed no evidence of cardiac dysfunction at 6 months but surprisingly demonstrated more severe hypertrophy after chronic pressure overload.²¹ Furthermore, it has been reported that MFN2-deficient mice display modest cardiac hypertrophy accompanied by slight functional deterioration.²² Reduction in either MFN1 or MFN2 can be partially compensated for by the other MFN protein, suggesting some overlap in function.²³ Knockout of either MFN1 or MFN2 was protective against ischemia/reperfusion injury in cardiomyocytes,^{22,24} whereas a combination knockout of MFN1/2 led to rapidly lethal cardiac failure.²⁵ The mitochondrial fission protein Drp1 has been linked to dilated cardiomyopathy.²⁶ OPA1 is the only protein known to mediate inner mitochondrial membrane fusion. Our previous work demonstrated a significant decrease of OPA1 protein content in both human and rat heart failure, whereas MFN1/2 surprisingly increased in human heart failure.⁸ In the current study, OPA1 mutation led to cardiomyopathy without changing the gene and protein level of MFN1/2 (Table S2 and Figure 7). These results suggest a unique role of OPA1 in regulating mitochondrial fusion, and depressed mitochondrial fusion may play a critical role in the downward progression of cardiomyopathies.

Decreased ATP production in OPA1-mutant hearts is likely a major factor in the decreased function, as demonstrated by echocardiography and hemodynamics. Depressed cardiomyocyte

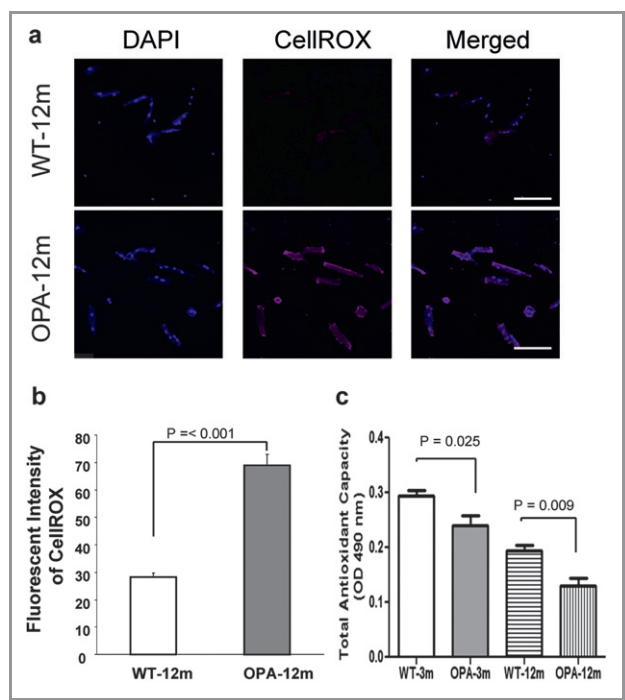


Figure 8. Reactive oxygen species (ROS) accumulated in OPA1-mutant hearts. a, Confocal microscopy image showing ROS accumulated in 12-month OPA1-mutant cardiomyocytes ($n=4$ donors per group). ROS was detected by a fluorogenic probe, CellROX Deep Red reagent. Nuclei stained with DAPI. Bar=100 μm . b, Summary of ROS intensity data from multiple experiments. c, Total antioxidant capacity measured in WT and OPA1-mutant left ventricles ($n=5$ per group). WT indicates wild type; OPA, OPA1^{+/-}; 3 m, 3 to 4 months; 12 m, 12 to 14 months. Data are represented as mean \pm SEM, and the *t* test was used to calculate statistical significance.

contractility and calcium transients may also partly result from the depressed ATP levels. To further understand the mechanism linking OPA1 to ATP generation, we measured mitochondrial oxygen consumption in the OPA1-mutant hearts. OCR decreased significantly in the OPA1-mutant cardiac mitochondria at 12 months. This is not surprising, as there are reports demonstrating a direct correlation between mitochondrial fusion and oxidative phosphorylation capacity.²⁷ Inhibition of mitofusins-mediated mitochondrial fusion in skeletal muscle,¹³ fibroblasts,²⁸ and MEFs²³ results in reduced oxygen consumption. The depressed OCR suggested electron transport chain (ETC) dysfunction, and this was confirmed by in vitro enzyme activity assays demonstrating that complex I and complex IV had decreased activity, whereas complex II activity was normal. This result is consistent with our finding of decreased COX activity (complex IV) by staining.

Although the pancreas-specific knockout of OPA1 does not affect mtDNA copy number,²⁹ our results demonstrate convincing loss of mtDNA copies in both young and older OPA1-mutant hearts. There is one theory that mitochondrial

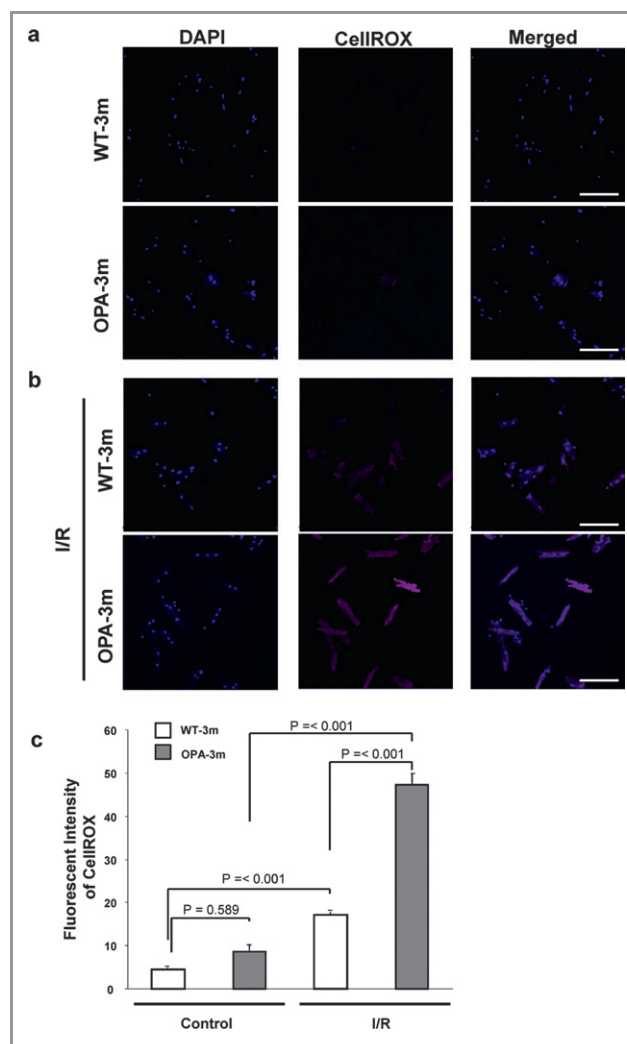


Figure 9. Reactive oxygen species (ROS) measured in young OPA1-mutant cardiomyocytes. a, ROS are undetectable in either WT or OPA1^{+/-} cardiomyocytes in the basal state. b, ROS after 1 hour of simulated ischemia with 1 hour of reoxygenation. c, Summary of ROS intensity data from multiple experiments. ROS were detected by a fluorogenic probe, CellROX Deep Red reagent ($n=4$ donors per group). Nuclei were stained with DAPI. Bar=100 μm . WT indicates wild type; OPA, OPA1^{+/-}; 3 m: 3 to 4 months; I/R, ischemia/reoxygenation. Data are represented as mean \pm SEM, and ANOVA was used to calculate statistical significance.

fusion/fission serves as a means of distribution of mtDNA to the progeny of mammalian cells,³⁰ which is supported by experiments demonstrating that the loss of mitofusins leads to loss of mtDNA in muscle.¹³ Recently, Elachouri et al found that silencing of OPA1 leads to mtDNA depletion, secondary to inhibition of mtDNA replication.³¹ In a series of clinical studies, specific OPA1 mutations were observed to induce the accumulation of mtDNA deletions in the skeletal muscle of patients.^{32,33} Altogether these observations suggested that altering mitochondrial dynamics affects the maintenance of mtDNA integrity. The loss of mtDNA induced by OPA1

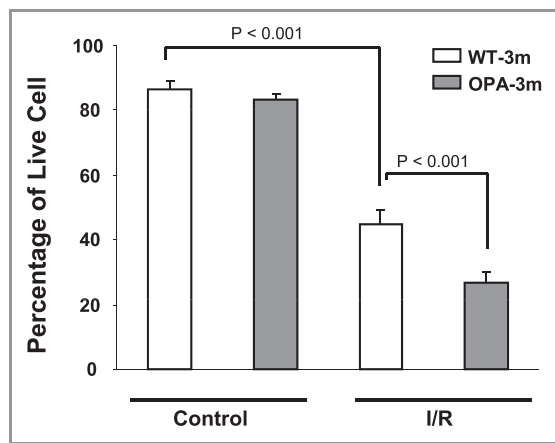


Figure 10. Cardiomyocyte viability after simulated ischemia followed by reoxygenation. Decreased OPA^{+/-}-cardiomyocyte viability after 6 hours of simulated ischemia and 1 hour of reoxygenation measured by a Live/Dead Viability Kit, in which green-fluorescent calcein-AM indicates live cells and red-fluorescent ethidium homodimer-1 indicates dead cells with loss of plasma membrane integrity. Percentage of live cardiomyocytes was calculated (n=4 donors per group). WT indicates wild type; OPA, OPA1^{+/-}; 3 m, 3 to 4 months; I/R, ischemia/reoxygenation. Data are represented as mean±SEM, and ANOVA was used to calculate statistical significance.

mutation may be the key factor in the development of cardiac mitochondrial dysfunction.

The mitochondrial fusion proteins OPA1 and MFN1/2 have been shown to protect cells from apoptosis. Increased fission, decreased fusion, or both can induce caspase activation, Bax translocation to mitochondria, and cytochrome c release.¹⁹ Bak may also regulate apoptosis by interacting with the

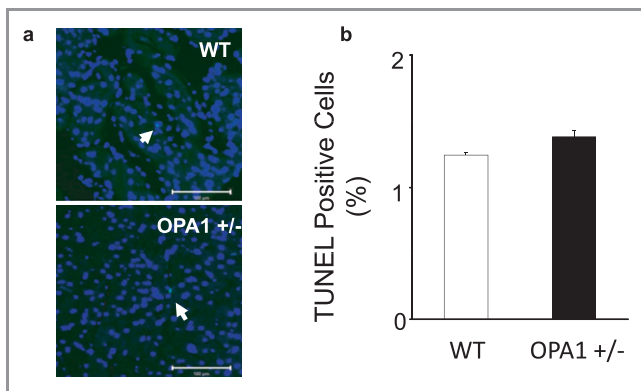


Figure 11. Apoptosis at 12 months. a, Representative confocal images of TUNEL-positive cells in left ventricle sections by TUNEL. Green fluorescence indicates TUNEL-positive apoptotic nuclei, with DAPI as a nuclear counter stain. b, Percentage of apoptotic cardiomyocytes was calculated based on TUNEL-positive fluorescence of cardiac myocytes/total cardiac myocytes (n=3 donors per group). Data are represented as mean±SEM, and the *t* test was used to calculate statistical significance.

mitofusins.³⁴ Interestingly, Bax may also positively regulate mitochondrial fusion exclusively through homotypic MFN2 trans complexes.³⁵ However, most of these results were generated in cultured cells. Even though our data from a myocytelike cell line indicates reduction of OPA1 induces apoptosis,⁸ we did not detect an increase in TUNEL-positive apoptotic myocytes in mouse left ventricular sections. Furthermore, we did not find changes in Bax or Bak expression in OPA1-mutant hearts. Thus, the mechanism of decreased cardiac function in the OPA1 mutant is not an increase in apoptosis. A similar conclusion was reached in an *in vivo* study in the pancreas,²⁹ where no increase in apoptosis associated with pancreas-specific knockout of OPA1.

OPA1 mutation-related cardiomyopathy was associated with increased ROS generation. Decreased mitochondrial ETC complex activity and mtDNA depletion may have contributed to this ROS accumulation. The accumulated ROS could also damage the ETC and mtDNA, creating a vicious cycle of damage. We were surprised to find marked depression of expression of a number of nuclear-encoded antioxidant genes, which would further exacerbate the ROS damage. The protein content of Nrf2, a transcription factor inducing expression of several antioxidant enzymes, was unchanged in OPA1-mutant hearts (Figure 7). The link between reduced OPA1 and reduced nuclear transcription will need to be addressed in future studies. Although there is no marked cardiac dysfunction evident in OPA1 mutants at 3 to 4 months, the decreased mtDNA copy number and increased ROS accumulation in these functionally “normal” hearts are evidence of significant abnormality despite normal function.

Mitochondrial morphologic abnormalities are associated with different types of cardiomyopathy^{8,36} in which OPA1 may be involved. Further work will be needed to fully define the role of abnormal mitochondrial fission/fusion in heart failure. The contribution of unbalanced mitochondrial fusion/fission to heart failure as a cause of myocardial injury remains to be proven. Nevertheless, the restoration of mitochondrial fusion/fission symmetry may help to rescue the failing heart. Treatment of adult murine cardiac myocytes with mitochondrial division inhibitor-1, a pharmacological inhibitor of Drp1, reduced cell death and infarct size after ischemia/reperfusion injury.³⁷ No cardiac disorders have been described in patients with OPA1 or similar mutations involving the fission/fusion genes as seen in inherited maladies like Charcot–Marie–Tooth disease. Our results indicate that, at least for OPA1, cardiac abnormalities are not completely manifest until the development of blindness. Although the OPA1-mutant mice survived more than 1 year and appeared healthy, we cannot exclude the changes in other organs had an effect on cardiac function, though this is unlikely. Thus, in patients with these diseases, reduced cardiac function may go undetected secondary to

reduced physical activity secondary to loss of vision. It would be expected that patients with such mutations would have impaired cardiac reserve with reduced ability to respond to high-stress disease states such as myocardial infarction and sepsis. The OPA1-mutant mice have reduced cardiac reserve, as shown by the lack of response to isoproterenol or to ischemia/reperfusion injury, as shown in the current study, suggesting that patients with OPA1 and related inherited mitochondrial diseases should be screened for abnormalities of cardiac function.

Sources of Funding

This study was supported by the National Institutes of Health (grant numbers HL077281 and HL079071, both to Dr Knowlton) and a Veterans Affairs Merit Award (to Dr Knowlton).

Disclosures

None.

References

- Liesa M, Palacin M, Zorzano A. Mitochondrial dynamics in mammalian health and disease. *Physiol Rev*. 2009;89:799–845.
- Chen H, Chan DC. Physiological functions of mitochondrial fusion. *Ann NY Acad Sci*. 2010;1201:21–25.
- Legros F, Lombès A, Frachon P, Rojo M. Mitochondrial fusion in human cells is efficient, requires the inner membrane potential, and is mediated by mitofusins. *Mol Biol Cell*. 2002;13:4343–4354.
- Chen H, Chan DC. Mitochondrial dynamics – fusion, fission, movement, and mitophagy – in neurodegenerative diseases. *Hum Mol Genet*. 2009;18:R169–R176.
- Zuchner S, Mersiyanova IV, Muglia M, Bissar-Tadmouri N, Rochelle J, Dadali EL, Zappia M, Nelis E, Patitucci A, Senderek J, Parman Y, Evgrafov O, Jonghe PD, Takahashi Y, Tsuji S, Pericak-Vance MA, Quattrone A, Battalouglu E, Polyakov AV, Timmerman V, Schroder JM, Vance JM. Mutations in the mitochondrial GTPase mitofusin 2 cause Charcot-Marie-Tooth neuropathy type 2A. *Nat Genet*. 2004;36:449–451.
- Alexander C, Votruba M, Pesch U, Thiselton D, Mayer S, Moore A, Rodriguez M, Kellner U, Leo-Kottler B, Auburger G, Bhattacharya S, Wissinger B. OPA1, encoding a dynamin-related GTPase, is mutated in autosomal dominant optic atrophy linked to chromosome 3q28. *Nat Genet*. 2000;26:211–215.
- Delettre C, Lenaers G, Griffioen JM, Gigarel N, Lorenzo C, Belenguer P, Pelloquin L, Grosgeorge J, Turc-Carel C, Perret E, Astarie-Dequeker C, Lasquelléc L, Arnaud B, Ducommun B, Kaplan J, Hamel CP. Nuclear gene OPA1, encoding a mitochondrial dynamin-related protein, is mutated in dominant optic atrophy. *Nat Genet*. 2000;26:207–210.
- Chen L, Gong Q, Stice JP, Knowlton AA. Mitochondrial OPA1, apoptosis, and heart failure. *Cardiovasc Res*. 2009;84:91–99.
- Davies VJ, Hollins AJ, Piechota MJ, Yip W, Davies JR, White KE, Nicols PP, Boulton ME, Votruba M. OPA1 deficiency in a mouse model of autosomal dominant optic atrophy impairs mitochondrial morphology, optic nerve structure and visual function. *Hum Mol Genet*. 2007;16:1307–1318.
- Xu D, Li N, He Y, Timofeyev V, Lu L, Tsai H-J, Kim I-H, Tuteja D, Mateo RKP, Singapurri A, Davis BB, Low R, Hammock BD, Chiamvimonvat N. Prevention and reversal of cardiac hypertrophy by soluble epoxide hydrolase inhibitors. *Proc Natl Acad Sci USA*. 2006;103:18733–18738.
- Kohout TA, Takaoka H, McDonald PH, Perry SJ, Mao L, Lefkowitz RJ, Rockman HA. Augmentation of cardiac contractility mediated by the human β 3-adrenergic receptor overexpressed in the hearts of transgenic mice. *Circulation*. 2001;104:2485–2491.
- Lu X-Y, Chen L, Cai X-L, Yang H-T. Overexpression of heat shock protein 27 protects against ischaemia/reperfusion-induced cardiac dysfunction via stabilization of troponin I and T. *Cardiovasc Res*. 2008;79:500–508.
- Chen H, Vermulst M, Wang YE, Chomyn A, Prolla TA, McCaffery JM, Chan DC. Mitochondrial fusion is required for mtDNA stability in skeletal muscle and tolerance of mtDNA mutations. *Cell*. 2010;141:280–289.
- Sahin E, Colla S, Liesa M, Moselehi J, Muller FL, Guo M, Cooper M, Kotton D, Fabian AJ, Walkey C, Maser RS, Tonon G, Foerster F, Xiong R, Wang YA, Shukla SA, Jaskelioff M, Martin ES, Heffernan TP, Protopopov A, Ivanova E, Mahoney JE, Kost-Altomova M, Perry SR, Bronson R, Liao R, Mulligan R, Shirihai OS, Chin L, DePinho RA. Telomere dysfunction induces metabolic and mitochondrial compromise. *Nature*. 2011;470:359–365.
- Li Q, Vande Velde C, Israelson A, Xie J, Bailey AO, Dong M-Q, Chun S-J, Roy T, Winer L, Yates JR, Capaldi RA, Cleveland DW, Miller TM. ALS-linked mutant superoxide dismutase 1 (SOD1) alters mitochondrial protein composition and decreases protein import. *Proc Natl Acad Sci USA*. 2010;107:21146–21151.
- Gao H, Chen L, Yang H-T. Activation of α 1b-adrenoceptors alleviates ischemia/reperfusion injury by limitation of mitochondrial Ca²⁺ overload in cardiomyocytes. *Cardiovasc Res*. 2007;75:584–595.
- Kelly DP. Cell biology: ageing theories unified. *Nature*. 2011;470:342–343.
- Reeve AK, Krishnan KJ, Turnbull D. Mitochondrial DNA mutations in disease, aging, and neurodegeneration. *Ann NY Acad Sci*. 2008;1147:21–29.
- Lee YJ, Jeong SY, Karbowski M, Smith CL, Youle RJ. Roles of the mammalian mitochondrial fission and fusion mediators Fis1, Drp1, and Opa1 in apoptosis. *Mol Biol Cell*. 2004;15:5001–5011.
- Dorn GW II, Clark CF, Eschenbacher WH, Kang MY, Engelhard JT, Warner SJ, Matkovich SJ, Jowdy CC. MARF and Opa1 control mitochondrial and cardiac function in Drosophila. *Circ Res*. 2011;108:12–17.
- Piquereau J, Caffin F, Novotova M, Prola A, Garnier A, Mateo P, Fortin D, Huynh LH, Nicolas V, Alavi MV, Brenner C, Ventura-Clapier R, Veksler V, Joubert F. Down-regulation of OPA1 alters mouse mitochondrial morphology, PTP function, and cardiac adaptation to pressure overload. *Cardiovasc Res*. 2012;94:408–417.
- Papanicolaou KN, Khairallah RJ, Ngoh GA, Chikando A, Luptak I, O'Shea KM, Riley DD, Lugus JJ, Colucci WS, Lederer WJ, Stanley WC, Walsh K. Mitofusin-2 maintains mitochondrial structure and contributes to stress-induced permeability transition in cardiac myocytes. *Mol Cell Biol*. 2011;31:1309–1328.
- Chen H, Chomyn A, Chan DC. Disruption of fusion results in mitochondrial heterogeneity and dysfunction. *J Biol Chem*. 2005;280:26185–26192.
- Papanicolaou KN, Ngoh GA, Dabkowski ER, O'Connell KA, Ribeiro RF, Stanley WC, Walsh K. Cardiomyocyte deletion of mitofusin-1 leads to mitochondrial fragmentation and improves tolerance to ROS-induced mitochondrial dysfunction and cell death. *Am J Physiol Heart Circ Physiol*. 2012;302:H167–H179.
- Chen Y, Liu Y, Dorn GW II. Mitochondrial fusion is essential for organelle function and cardiac homeostasis. *Circ Res*. 2011;109:1327–1331.
- Ashrafian H, Docherty L, Leo V, Towson C, Neilan M, Steeples V, Lygate CA, Hough T, Townsend S, Williams D, Wells S, Norris D, Glyn-Jones S, Land J, Barbaric I, Lalanne Z, Denny P, Szumska D, Bhattacharya S, Griffin JL, Hargreaves I, Fernandez-Fuentes N, Cheeseman M, Watkins H, Dear TN. A mutation in the mitochondrial fission gene Dnm1l leads to cardiomyopathy. *PLoS Genet*. 2010;6:e1001000.
- Zanna C, Ghelli A, Porcelli AM, Karbowski M, Youle RJ, Schimpf S, Wissinger B, Pinti M, Cossarizza A, Vidoni S, Valentino ML, Rugolo M, Carelli V. OPA1 mutations associated with dominant optic atrophy impair oxidative phosphorylation and mitochondrial fusion. *Brain*. 2008;131:352–367.
- Bach D, Pich S, Soriano FX, Vega N, Baumgartner B, Oriola J, Daugaard JR, Lloberas J, Camps M, Zierath JR, Rabasa-Lhoret R, Wallberg-Henriksson H, Laville M, Palacin M, Vidal H, Rivera F, Brand M, Zorzano A. Mitofusin-2 determines mitochondrial network architecture and mitochondrial metabolism. *J Biol Chem*. 2003;278:17190–17197.
- Zhang Z, Wakabayashi N, Wakabayashi J, Tamura Y, Song W-J, Sereda S, Clerc P, Polster BM, Aja SM, Pletnikov MV, Kensler TW, Shirihai OS, Iijima M, Hussain MA, Sesaki H. The dynamin-related GTPase OPA1 is required for glucose-stimulated ATP production in pancreatic beta cells. *Mol Biol Cell*. 2011;22:2235–2245.
- Margineantu DH, Gregory Cox W, Sundell L, Sherwood SW, Beechem JM, Capaldi RA. Cell cycle dependent morphology changes and associated mitochondrial DNA redistribution in mitochondria of human cell lines. *Mitochondrion*. 2002;1:425–435.
- Elachouri G, Vidoni S, Zanna C, Pattyn A, Boukhaddaoui H, Gaget K, Yu-Wai-Man P, Gasparre G, Sarzi E, Delettre C, Olichon A, Loiseau D, Reynier P, Chinnery PF, Rotig A, Carelli V, Hamel CP, Rugolo M, Lenaers G. OPA1 links human mitochondrial genome maintenance to mtDNA replication and distribution. *Genome Res*. 2011;21:12–20.
- Hudson G, Amati-Bonneau P, Blakely EL, Stewart JD, He L, Schaefer AM, Griffiths PG, Ahlqvist K, Suomalainen A, Reynier P, McFarland R, Turnbull DM, Chinnery PF, Taylor RW. Mutation of OPA1 causes dominant optic atrophy with external ophthalmoplegia, ataxia, deafness and multiple mitochondrial DNA deletions: a novel disorder of mtDNA maintenance. *Brain*. 2008;131:329–337.

33. Amati-Bonneau P, Valentino ML, Reynier P, Gallardo ME, Bornstein B, Boissiere A, Campos Y, Rivera H, de la Aleja JG, Carroccia R, Iommarini L, Labauge P, Figarella-Branger D, Marcocelles P, Furby A, Beauvais K, Letournel F, Liguori R, La Morgia C, Montagna P, Liguori M, Zanna C, Rugolo M, Cossarizza A, Wissinger B, Verny C, Schwarzenbacher R, Martin MA, Arenas J, Ayuso C, Garesse R, Lenaers G, Bonneau D, Carelli V. Opa1 mutations induce mitochondrial DNA instability and optic atrophy 'plus' phenotypes. *Brain*. 2008;131:338–351.
34. Brooks C, Wei Q, Feng L, Dong G, Tao Y, Mei L, Xie ZJ, Dong Z. Bak regulates mitochondrial morphology and pathology during apoptosis by interacting with mitofusins. *Proc Natl Acad Sci USA*. 2007;104:11649–11654.
35. Hoppins S, Edlich F, Cleland MM, Banerjee S, McCaffery JM, Youle RJ, Nunnari J. The soluble form of Bax regulates mitochondrial fusion via MFN2 homotypic complexes. *Mol Cell*. 2011;41:150–160.
36. Hom J, Yu T, Yoon Y, Porter G, Sheu SS. Regulation of mitochondrial fission by intracellular Ca²⁺ in rat ventricular myocytes. *Biochim Biophys Acta*. 2010;1797:913–921.
37. Ong SB, Subrayan S, Lim SY, Yellon DM, Davidson SM, Hausenloy DJ. Inhibiting mitochondrial fission protects the heart against ischemia/reperfusion injury. *Circulation*. 2010;121:2012–2022.

Table S1: Transcriptional regulation of genes related to Oxidative Stress and Antioxidant Defense
RT² Profiler™ PCR Array Mouse Oxidative Stress and Antioxidant Defense (PAMM-065A)

Gene	Description	Fold induction	P value	q value	Fold induction	P value	q value
		OPAI +/- vs. WT (3-4 months)			OPAI +/- vs. WT (12 months)		
Gpx8	Glutathione peroxidase 8 (putative)	-1.43	0.36	0.37	1.03	0.84	0.37
Aass	Aminoacidipate-semialdehyde synthase	1.16	0.61	0.41	2.23	0.50	0.35
Als2	Amyotrophic lateral sclerosis 2 (juvenile) homolog (human)	-1.38	0.41	0.37	-1.79	0.20	0.35
Apc	Adenomatosis polyposis coli	1.89	0.10	0.34	1.41	0.57	0.35
Apoe	Apolipoprotein E	-1.29	0.65	0.41	-1.27	0.56	0.35
Aqr	Aquarius	-1.26	0.48	0.38	-1.36	0.12	0.35
Atr	Ataxia telangiectasia and rad3 related	1.19	0.95	0.52	-1.42	0.38	0.35
Cat	Catalase	1.33	0.27	0.34	-1.29	0.47	0.35
Ccs	Copper chaperone for superoxide dismutase	1.08	0.63	0.41	-1.23	0.56	0.35
Xirp1	Xin actin-binding repeat containing 1	-1.84	0.47	0.38	-2.10	0.11	0.35
Ctsb	Cathepsin B	1.44	0.34	0.36	1.54	0.56	0.35
Cyba	Cytochrome b-245, alpha polypeptide	-1.53	0.40	0.37	-1.31	0.03	0.26
Cygb	Cytoglobin	-1.58	0.46	0.38	-1.14	0.76	0.35
Dnm2	Dynamin 2	1.76	0.27	0.34	-1.23	0.56	0.35
Duox1	Dual oxidase 1	-1.72	0.72	0.44	-1.70	0.37	0.35
Ehd2	EH-domain containing 2	-2.05	0.26	0.34	-2.47	0.22	0.35
Epx	Eosinophil peroxidase	-1.35	0.43	0.37	-1.65	0.46	0.35
Ercc2	Excision repair cross-complementing rodent repair deficiency, complementation group 2	-1.34	0.75	0.45	-2.19	0.32	0.35
Ercc6	Excision repair cross-complementing rodent repair deficiency, complementation group 6	1.88	0.04	0.34	1.74	0.30	0.35
Fancc	Fanconi anemia, complementation group C	-1.16	0.49	0.38	-1.14	0.73	0.35
Fmo2	Flavin containing monooxygenase 2	-2.37	0.09	0.34	-1.60	0.25	0.35
Gab1	Growth factor receptor bound protein 2-associated protein 1	-1.82	0.25	0.34	-1.93	0.49	0.35
Gpx1	Glutathione peroxidase 1	1.28	0.99	0.52	1.16	0.75	0.35
Gpx2	Glutathione peroxidase 2	-3.34	0.01	0.34	-1.38	0.51	0.35
Gpx3	Glutathione peroxidase 3	-3.10	0.04	0.34	-2.67	0.01	0.25
Gpx4	Glutathione peroxidase 4	-1.81	0.15	0.34	-1.47	0.28	0.35
Gpx5	Glutathione peroxidase 5	-1.37	0.31	0.34	1.35	0.70	0.35
Gpx6	Glutathione peroxidase 6	-1.49	0.26	0.34	-1.02	0.66	0.35
Gpx7	Glutathione peroxidase 7	-1.40	0.27	0.34	-1.85	0.51	0.35
Gsr	Glutathione reductase	-2.05	0.11	0.34	-1.64	0.50	0.35
Gstk1	Glutathione S-transferase kappa 1	-2.16	0.04	0.34	-1.63	0.02	0.26
Hbq1	Hemoglobin, theta 1	1.05	0.85	0.48	1.22	0.93	0.39
Idh1	Isocitrate dehydrogenase 1 (NADP+), soluble	-1.80	0.08	0.34	-1.99	0.34	0.35
Ift172	Intraflagellar transport 172 homolog (Chlamydomonas)	-1.23	0.25	0.34	-1.68	0.35	0.35
Il19	Interleukin 19	-2.67	0.22	0.34	-1.36	0.71	0.35
Il22	Interleukin 22	1.13	0.77	0.45	-1.12	0.72	0.35
Kif9	Kinesin family member 9	1.41	0.54	0.39	-1.09	0.66	0.35
Lpo	Lactoperoxidase	-1.75	0.16	0.34	-1.20	0.59	0.35
Mb	Myoglobin	1.31	0.62	0.41	1.50	0.27	0.35
Mpo	Myeloperoxidase	-4.67	0.42	0.37	1.84	0.87	0.37
Mpp4	Membrane protein, palmitoylated 4 (MAGUK p55 subfamily member 4)	-1.37	0.31	0.34	1.35	0.70	0.35
Ncf2	Neutrophil cytosolic factor 2	1.09	0.92	0.51	-1.26	0.32	0.35
Ngb	Neuroglobin	-1.78	0.15	0.34	1.35	0.70	0.35
Nos2	Nitric oxide synthase 2, inducible	1.60	0.81	0.46	2.40	0.41	0.35
Nox1	NADPH oxidase 1	-2.36	0.06	0.34	-1.78	0.36	0.35
Nox4	NADPH oxidase 4	-2.53	0.13	0.34	-1.08	0.79	0.36
Noxa1	NADPH oxidase activator 1	-1.49	0.27	0.34	1.25	0.69	0.35
Noxo1	NADPH oxidase organizer 1	1.13	0.68	0.43	-1.45	0.58	0.35

Nqo1	NAD(P)H dehydrogenase, quinone 1	1.24	0.48	0.38	1.16	0.98	0.40
Nudt15	Nudix (nucleoside diphosphate linked moiety X)-type motif 15	-2.48	0.11	0.34	-1.60	0.51	0.35
Nxn	Nucleoredoxin	1.45	0.61	0.41	1.36	0.64	0.35
Park7	Parkinson disease (autosomal recessive, early onset) 7	-1.41	0.28	0.34	-2.45	0.13	0.35
Ppp1r15b	Protein phosphatase 1, regulatory (inhibitor) subunit 15b	-1.19	0.56	0.39	-1.16	0.52	0.35
Prdx1	Peroxiredoxin 1	1.41	0.27	0.34	1.12	0.64	0.35
Prdx2	Peroxiredoxin 2	-1.21	0.56	0.39	-2.33	0.05	0.33
Prdx3	Peroxiredoxin 3	1.24	0.81	0.46	1.07	0.74	0.35
Prdx4	Peroxiredoxin 4	1.22	0.99	0.52	1.46	0.47	0.35
Prdx5	Peroxiredoxin 5	-3.57	0.11	0.34	-2.53	0.11	0.35
Prdx6	Peroxiredoxin 6	-1.96	0.18	0.34	-1.64	0.18	0.35
Prdx6-rs1	Peroxiredoxin 6, related sequence 1	-4.21	0.25	0.34	-3.41	0.02	0.26
Prnp	Prion protein	-1.83	0.30	0.34	-2.52	0.21	0.35
Psmb5	Proteasome (prosome, macropain) subunit, beta type 5	-1.15	0.56	0.39	-1.46	0.30	0.35
Ptgs1	Prostaglandin-endoperoxide synthase 1	-1.89	0.12	0.34	-1.27	0.35	0.35
Ptgs2	Prostaglandin-endoperoxide synthase 2	-2.34	0.37	0.37	-1.15	0.65	0.35
Rag2	Recombination activating gene 2	-1.84	0.13	0.34	-1.49	0.59	0.35
Recq4	RecQ protein-like 4	1.14	0.49	0.38	1.46	0.73	0.35
Scd1	Stearoyl-Coenzyme A desaturase 1	-1.60	0.42	0.37	-1.55	0.22	0.35
Serp1nb1b	Serine (or cysteine) peptidase inhibitor, clade B, member 1b	-1.33	0.49	0.38	1.70	0.26	0.35
Slc38a1	Solute carrier family 38, member 1	-1.17	0.56	0.39	2.14	0.31	0.35
Slc41a3	Solute carrier family 41, member 3	1.60	0.41	0.37	-1.24	0.47	0.35
Sod1	Superoxide dismutase 1, soluble	11.38	0.74	0.45	-1.61	0.39	0.35
Sod2	Superoxide dismutase 2, mitochondrial	2.68	0.40	0.37	1.04	0.69	0.35
Sod3	Superoxide dismutase 3, extracellular	-1.81	0.32	0.34	-1.91	0.12	0.35
Srxn1	Sulfiredoxin 1 homolog (<i>S. cerevisiae</i>)	-1.95	0.22	0.34	-2.63	0.04	0.29
Tmod1	Tropomodulin 1	-2.02	0.19	0.34	-1.57	0.45	0.35
Tpo	Thyroid peroxidase	-2.79	0.13	0.34	-2.24	0.39	0.35
Txnip	Thioredoxin interacting protein	2.29	0.03	0.34	1.04	0.86	0.37
Txnrd1	Thioredoxin reductase 1	-1.97	0.99	0.52	-1.36	0.47	0.35
Txnrd2	Thioredoxin reductase 2	-5.01	0.05	0.34	-1.41	0.47	0.35
Txnrd3	Thioredoxin reductase 3	-8.71	0.65	0.41	1.09	0.87	0.37
Ucp3	Uncoupling protein 3 (mitochondrial, proton carrier)	2.40	0.11	0.34	-1.14	0.58	0.35
Vim	Vimentin	-1.06	0.77	0.45	1.72	0.42	0.35
Xpa	Xeroderma pigmentosum, complementation group A	6.14	0.95	0.52	1.12	0.84	0.37
Zmynd17	Zinc finger, MYND domain containing 17	-1.16	0.52	0.39	1.05	0.99	0.40

Positive value = up-regulation; negative value = down-regulation.

Table S2: Transcriptional regulation of key genes related mitochondria (12 months)

Gene	Description	Fold induction	P value	q value
Aifm2	Apoptosis-inducing factor, mitochondrion-associated 2	1.08	0.92	0.80
Aip	Aryl-hydrocarbon receptor-interacting protein	1.40	0.15	0.59
Bak1	BCL2-antagonist/killer 1	1.55	0.39	0.59
Bbc3	BCL2 binding component 3	2.70	0.38	0.59
Bcl2	B-cell leukemia/lymphoma 2	1.89	0.44	0.59
Bcl2l1	Bcl2-like 1	-2.81	0.15	0.59
Bid	BH3 interacting domain death agonist	1.52	0.52	0.61
Bnip3	BCL2/adenovirus E1B interacting protein 3	-1.63	0.16	0.59
Cdkn2a	Cyclin-dependent kinase inhibitor 2A	1.87	0.43	0.59
Cox10	COX10 homolog, cytochrome c oxidase assembly protein, heme A: farnesyltransferase (yeast)	-1.56	0.97	0.81
Cox18	COX18 cytochrome c oxidase assembly homolog (S. cerevisiae)	1.20	0.47	0.59
Cpt1b	Carnitine palmitoyltransferase 1b, muscle	-1.03	0.71	0.73
Cpt2	Carnitine palmitoyltransferase 2	1.28	0.56	0.63
Dnajc19	DnaJ (Hsp40) homolog, subfamily C, member 19	-1.25	0.91	0.80
Dnm1l	Dynamin 1-like	1.31	0.40	0.59
Fis1	Fission 1 (mitochondrial outer membrane) homolog (yeast)	1.08	0.65	0.69
Fxc1	Fractured callus expressed transcript 1	-1.29	0.75	0.74
Grpel1	GrpE-like 1, mitochondrial	1.30	0.27	0.59
Hsp90aa1	Heat shock protein 90, alpha (cytosolic), class A member 1	1.29	0.29	0.59
Hspd1	Heat shock protein 1 (chaperonin)	1.42	0.33	0.59
Immp1l	IMP1 inner mitochondrial membrane peptidase-like (S. cerevisiae)	1.32	0.35	0.59
Immp2l	IMP2 inner mitochondrial membrane peptidase-like (S. cerevisiae)	1.83	0.25	0.59
Lrpprc	Leucine-rich PPR-motif containing	-1.05	0.94	0.80
Mfn1	Mitofusin 1	1.49	0.44	0.59
Mfn2	Mitofusin 2	1.20	0.54	0.62
Mipep	Mitochondrial intermediate peptidase	1.13	0.54	0.62
Msto1	Misato homolog 1 (Drosophila)	-1.17	0.90	0.80
Mtx2	Metaxin 2	1.05	0.67	0.70
Nefl	Neurofilament, light polypeptide	1.54	0.44	0.59
Opa1	Optic atrophy 1 homolog (human)	-2.23	0.01	0.59
Pmaip1	Phorbol-12-myristate-13-acetate-induced protein 1	2.17	0.47	0.59
Rhot1	Ras homolog gene family, member T1	1.85	0.37	0.59
Rhot2	Ras homolog gene family, member T2	-1.05	0.84	0.79
Sfn	Stratifin	2.74	0.45	0.59
Sh3glb1	SH3-domain GRB2-like B1 (endophilin)	1.42	0.44	0.59
Slc25a1	Solute carrier family 25 (mitochondrial carrier, citrate transporter), member 1	1.75	0.31	0.59
Slc25a10	Solute carrier family 25 (mitochondrial carrier, dicarboxylate transporter), member 10	2.43	0.22	0.59
Slc25a12	Solute carrier family 25 (mitochondrial carrier, Aralar), member 12	-1.77	0.34	0.59
Slc25a13	Solute carrier family 25 (mitochondrial carrier, adenine nucleotide translocator), member 13	1.63	0.24	0.59
Slc25a14	Solute carrier family 25 (mitochondrial carrier, brain), member 14	1.46	0.37	0.59
Slc25a15	Solute carrier family 25 (mitochondrial carrier ornithine transporter), member 15	1.63	0.38	0.59
Slc25a16	Solute carrier family 25 (mitochondrial carrier, Graves disease autoantigen), member 16	1.82	0.11	0.59
Slc25a17	Solute carrier family 25 (mitochondrial carrier, peroxisomal membrane protein), member 17	1.30	0.39	0.59
Slc25a19	Solute carrier family 25 (mitochondrial thiamine pyrophosphate carrier), member 19	1.51	0.27	0.59

Slc25a2	Solute carrier family 25 (mitochondrial carrier, ornithine transporter) member 2	2.73	0.33	0.59
Slc25a20	Solute carrier family 25 (mitochondrial carnitine/acylcarnitine translocase), member 20	-1.03	0.84	0.79
Slc25a21	Solute carrier family 25 (mitochondrial oxodicarboxylate carrier), member 21	5.01	0.41	0.59
Slc25a22	Solute carrier family 25 (mitochondrial carrier, glutamate), member 22	1.25	0.38	0.59
Slc25a23	Solute carrier family 25 (mitochondrial carrier; phosphate carrier), member 23	1.02	0.89	0.80
Slc25a24	Solute carrier family 25 (mitochondrial carrier, phosphate carrier), member 24	1.88	0.41	0.59
Slc25a25	Solute carrier family 25 (mitochondrial carrier, phosphate carrier), member 25	3.13	0.24	0.59
Slc25a27	Solute carrier family 25, member 27	1.43	0.38	0.59
Slc25a3	Solute carrier family 25 (mitochondrial carrier, phosphate carrier), member 3	-1.12	0.34	0.59
Slc25a30	Solute carrier family 25, member 30	1.73	0.43	0.59
Slc25a31	Solute carrier family 25 (mitochondrial carrier; adenine nucleotide translocator), member 31	3.42	0.43	0.59
Slc25a37	Solute carrier family 25, member 37	1.25	0.48	0.60
Slc25a4	Solute carrier family 25 (mitochondrial carrier, adenine nucleotide translocator), member 4	1.40	0.27	0.59
Slc25a5	Solute carrier family 25 (mitochondrial carrier, adenine nucleotide translocator), member 5	1.14	0.25	0.59
Sod1	Superoxide dismutase 1, soluble	-1.51	0.58	0.64
Sod2	Superoxide dismutase 2, mitochondrial	-1.11	0.84	0.79
Stard3	START domain containing 3	-1.27	0.93	0.80
Taz	Tafazzin	1.55	0.20	0.59
Timm10	Translocase of inner mitochondrial membrane 10 homolog (yeast)	-1.59	0.52	0.61
Timm17a	Translocase of inner mitochondrial membrane 17a	1.44	0.29	0.59
Timm17b	Translocase of inner mitochondrial membrane 17b	1.39	0.39	0.59
Timm22	Translocase of inner mitochondrial membrane 22 homolog (yeast)	1.24	0.12	0.59
Timm23	Translocase of inner mitochondrial membrane 23 homolog (yeast)	-1.22	0.63	0.69
Timm44	Translocase of inner mitochondrial membrane 44	1.39	0.16	0.59
Timm50	Translocase of inner mitochondrial membrane 50 homolog (yeast)	-1.03	0.72	0.73
Timm8a1	Translocase of inner mitochondrial membrane 8 homolog a1 (yeast)	1.00	0.84	0.79
Timm8b	Translocase of inner mitochondrial membrane 8 homolog b (yeast)	-1.06	0.92	0.80
Timm9	Translocase of inner mitochondrial membrane 9 homolog (yeast)	1.50	0.36	0.59
Tomm20	Translocase of outer mitochondrial membrane 20 homolog (yeast)	-1.10	0.92	0.80
Tomm22	Translocase of outer mitochondrial membrane 22 homolog (yeast)	1.26	0.45	0.59
Tomm34	Translocase of outer mitochondrial membrane 34	1.44	0.07	0.59
Tomm40	Translocase of outer mitochondrial membrane 40 homolog (yeast)	2.94	0.36	0.59
Tomm40l	Translocase of outer mitochondrial membrane 40 homolog-like (yeast)	1.18	0.49	0.60
Tomm70a	Translocase of outer mitochondrial membrane 70 homolog A (yeast)	1.56	0.19	0.59
Trp53	Transformation related protein 53	1.59	0.40	0.59
Tspo	Translocator protein	1.56	0.33	0.59
Ucp1	Uncoupling protein 1 (mitochondrial, proton carrier)	5.89	0.47	0.59
Ucp2	Uncoupling protein 2 (mitochondrial, proton carrier)	-1.30	0.99	0.82
Ucp3	Uncoupling protein 3 (mitochondrial, proton carrier)	-1.12	0.64	0.69
Uxt	Ubiquitously expressed transcript	1.24	0.36	0.59

Positive value = up-regulation; negative value = down-regulation.

Table S3: Primers used to identify mtDNA copy number.

Mitochondrial primers	
COXIF	CTGAGCGGGAATAGTGGGTA
COXIR	TGGGGCTCCGATTATTAGTG
CytBF	ATTCCTTCATGTCGGACGAG
CytBR	ACTGAGAAGCCCCCTCAAAT
Genomic primers	
H19R	GTCCACGAGACCAATGACTG
H19F	GTACCCACCTGTCGTCC
B1globinF	GCACCTGACTGATGCTGAGAA
B1globinR	TTCATCGGCGTTCACCTTCC